Int. Journal of Refractory Metals & Hard Materials 27 (2009) 996–1003

Contents lists available at ScienceDirect

Int. Journal of Refractory Metals & Hard Materials

journal homepage: www.elsevier.com/locate/IJRMHM

Wear-resistant ceramic and metal–ceramic ultrafine composites fabricated from combustion synthesised metastable powders

D. Vallauri [a,*], B. DeBenedetti [a], L. Jaworska [b], P. Klimczyk [b], M.A. Rodriguez [c]

[a] Dipartimento di Scienza dei Materiali e Ingegneria Chimica, Politecnico di Torino, Corso Duca degli Abruzzi 24, 10129 Torino, Italy
[b] Institute of Advanced Manufacturing Technology, Wroclawska 37a, 30-011 Cracow, Poland
[c] Instituto de Ceramica y Vidrio (CSIC), Campus de Cantoblanco, C/Kelsen 5, 28049 Madrid, Spain

ARTICLE INFO

Article history:
Received 24 March 2009
Accepted 10 July 2009

Keywords:
Ceramic composites
Cermets
High-pressure high-temperature sintering
Wear-resistance

ABSTRACT

Dense Ti–Al_2O_3–TiC cermet and TiC–TiB_2 ceramic composites have been fabricated by high-pressure high-temperature (HPHT) sintering starting from metastable nanostructured powders obtained by means of a technique based on the self-propagating high-temperature synthesis (SHS) process. The microstructural observations showed that an ultrafine microstructure was retained in the sintered composites thanks to the limited grain growth allowed by the short sintering duration of the HPHT method. The sintered TiC–TiB_2 and Ti–Al_2O_3–TiC fine-grained bulk composites exhibited high values of hardness and Young modulus. The tribological characterization confirmed the good properties of both the materials in terms of wear-resistance and makes them very promising candidates for demanding applications. The influence of the ultrafine grain size on physical and tribological properties of the densified materials is discussed.

1. Introduction

In the context of the design and processing of advanced materials to improve performance and durability of highly stressed components, the development of ceramic–ceramic and metal–ceramic composites is of increasing interest. These materials are in fact effective in enhancing the intrinsically low fracture toughness with the simultaneous improvement of the wear-resistance of monolithic ceramics [1,2].

The manufacture of nanocrystalline materials has been successfully achieved in the past in the case of binary oxide systems through processing routes based on metastable transformations [3], to obtain composite powders that are inherently metastable and nanostructured. In the case of previously unexplored non-oxide systems, the adoption of the metastability approach has been successfully set up for the achievement of nanostructured composite powders. The synthesis of TiC_{1-x}/TiB_2 [4] and Ti–Al_2O_3–TiC [5] nanostructured powders by means of an innovative metastability route based on the self-propagating high-temperature synthesis (SHS) process followed by quench was obtained. The stoichiometry of the reactant systems was optimized in order to have SHS reactions characterized by a combustion temperature higher than the eutectic temperature of the system. The rapid cooling by quench in liquid nitrogen of the SHS products immediately following the reaction yielded inherently nanostructured powder agglomerates. The SHS–quench process led to the formation of powder agglomerates characterized by fine structures [6], yielding nanopowders after milling.

Regarding the densification of the powders, the main problem in the consolidation of particulate nanostructured materials is the set up of a full compaction with retention of the nanocrystalline structure and the prevention of grain growth phenomena. The metastability route is such that, regardless of the phases formed after the process, a ceramic or metal–ceramic mixture can be converted into a stable two-phase structure after the consolidation treatment, in the form of either a dispersed phase in a matrix or of a bi-continuous nanocomposite [7]. The energy released during the transition from metastable to thermally-stable structures is capable of allowing the activation of the densification process through vacancy diffusion phenomena with a simultaneous grain growth inhibition due to the high-pressure exerted [8]. In fact, the highly strained structure can be easily annealed without appreciable grain growth (e.g. with an increase from 18 nm from the original metastable powder to 49 nm in the sintered compact, as reported in [7]) which is mutually suppressed by the near immiscibility of the constituent phases [9]. This allows to carry out the densification process at temperature lower than that used in the traditional processing. This concept can be applied to process the inherently metastable and nanostructured powders obtained by SHS + quench, that can be converted into a stable and ultrafine-grained composite microstructure upon recrystallisation by medium temperature treatments [10].

* Corresponding author. Tel.: +39 011 5644672; fax: +39 011 5644699.
E-mail address: dario.vallauri@polito.it (D. Vallauri).

0263-4368/$ - see front matter © 2009 Elsevier Ltd. All rights reserved.
doi:10.1016/j.ijrmhm.2009.07.003

The purpose of the present work was the densification of the nanostructured TiC_{1-x}–TiB_2 and Ti–Al_2O_3–TiC powders produced by SHS + quench by means of high-pressure high-temperature (HPHT) sintering to obtain dense ultrafine ceramics and cermets. Due to the short sintering duration, the HPHT method is suitable to allow the recrystallization process and simultaneously limit the grain growth. The wear behavior of the densified materials was studied using a ball-on-disk tribometer and the predominant wear mechanisms are discussed.

2. Experimental activity

A common procedure was set up for the fabrication of wear-resistant materials, based on the synthesis of the two compositions (TiC_{1-x}–TiB_2 ceramic composite and Ti–Al_2O_3–TiC cermet) followed by consolidation of the synthesized powders.

Concerning the synthesis of the powders, a specific process based on the metastability concept has been designed and set up in order to synthesise the TiC_{1-x}–TiB_2 eutectic composition and the Ti–Al_2O_3–TiC cermet through SHS [11] followed by quench into a liquid nitrogen bath. The SHS + quench experiments were carried out in a purposely designed vessel filled with flowing argon gas at atmospheric pressure. The detailed procedure for the powder synthesis is reported in [5] for the Ti–Al_2O_3–TiC cermet and in [6] for the TiC_{1-x}–TiB_2 ceramic system.

In the case of the Ti–Al_2O_3–TiC cermet, a titanium enriched composition was selected and a mixture of titanium and carbon was added as booster. This was due to the fact that the stoichiometric reaction (60 wt.% Ti/40 wt.% Al_2O_3) was not self-sustained. The detailed procedure followed for the optimisation of the stoichiometry of the SHS reaction is reported in [5]. The optimized final composition was 13 wt.% of TiC, 53 wt.% of titanium and 35 wt.% of alumina. Regarding the ceramic TiC–TiB_2 material, the stoichiometry of the reactant mixture was optimized to yield products with eutectic composition, corresponding to approximately 62 wt.% of titanium carbide and 38 wt.% of titanium diboride (i.e. 67 mol% TiC/33 mol% TiB_2).

The products of the two reactions were subjected to hand-crushing in a mortar and then milled in an attritor mill with zircona balls for the Ti–Al_2O_3–TiC cermet and WC-Co balls for the TiC–TiB_2 ceramic (ball-to-powder relation of 2.2 vol.) in isopropilic alcohol to a particle size finer than 10 μm. The TiC–TiB_2 and Ti–Al_2O_3–TiC SHS–quenched powder products were then dried for 2 h at approximately 150 °C and shaped into discs (ϕ = 15 mm, h = 5.5 mm, green density ≅ 3 g/cm^3) by cold pressing in a steel die under a pressure of 200 MPa. The green samples were consolidated by HPHT sintering using a toroidal Bridgmann type apparatus provided with an internal graphite heater, shown in Fig. 1.

The main criteria for the optimisation of the HPHT sintering conditions (pressure, temperature, duration) were the evaluation of density, Young modulus and hardness of the sintered compacts. Two values of compaction pressure were tested, namely 4 GPa and 7.7 GPa. The sintering temperature ranged between 1070 °C and 2370 °C. The duration of the sintering cycle was varied between 30 s and 240 s. The density of the densified samples were measured by hydrostatic method. Young modulus was measured based on the velocity of ultrasonic waves transition through the sintered samples using an ultrasonic flaw detector Panametrics Epoch III. The hardness of the HPHT samples was determined by Vickers method using a Vickers Hardness Tester FUTURE-TECH FV-700. The fracture toughness was calculated using Niihara equation [12] from the length of the cracks developed after the Vickers indentation test. The values reported in this paper are an average of at least 6 measurements. The sintered samples were characterized by X-ray diffraction by means of a Philips X'Pert Pro diffractometer with a Cu kα radiation (λ = 0.154060 nm). The crystallite size of the final phases was estimated based on X-ray line broadening (FWHM – full width on half maximum) using the Rietveld refinement method. Microstructural observations were carried out on the densified materials by scanning electron microscopy in a LEO SUPRA 40 Field–Emission Scanning Electron Microscope (FESEM) equipped with back scattering electron (BSE) detector and EDS/EDAX microprobe. The wear behavior of the HPHT materials was evaluated by ball-on-disk wear tests. According to this method, the sliding contact is brought by pushing a ball specimen onto a rotating disc specimen under a constant load. The disk was made of either TiC–TiB_2 or Ti–Al_2O_3–TiC sintered material. Disks with diameter ~13.5 mm and height ~4.5 mm and a Si_3N_4 ball with diameter 1 mm were used. During the wear tests, the coefficient of friction μ of the tested material, temperature in the ball-disk contact zone were measured and the specific wear rate according to wear volume was determined. The tests were carried out without lubricant according to the ISO 20808:2004(E). Because of the HPHT compacts size limitation the following parameters were established: applied load 1 N, sliding speed 0.1 m/s, diameter of the sliding circle 5 mm, sliding distance 100 m, number of cycles 3200. The thermal shock resistance of the TiC–TiB_2 and Ti–Al_2O_3–TiC sintered materials was evaluated by means of thermal shock tests through quenching into water according to the EN 820-3:2004 standard. The development of surface cracks after the thermal shock tests was investigated on the tested samples using a scanning microscope Jeol JSM-6460LV. In the case of sample cracking, the test was repeated with fresh samples at a lower temperature. The procedure was continued until the occurrence of surface

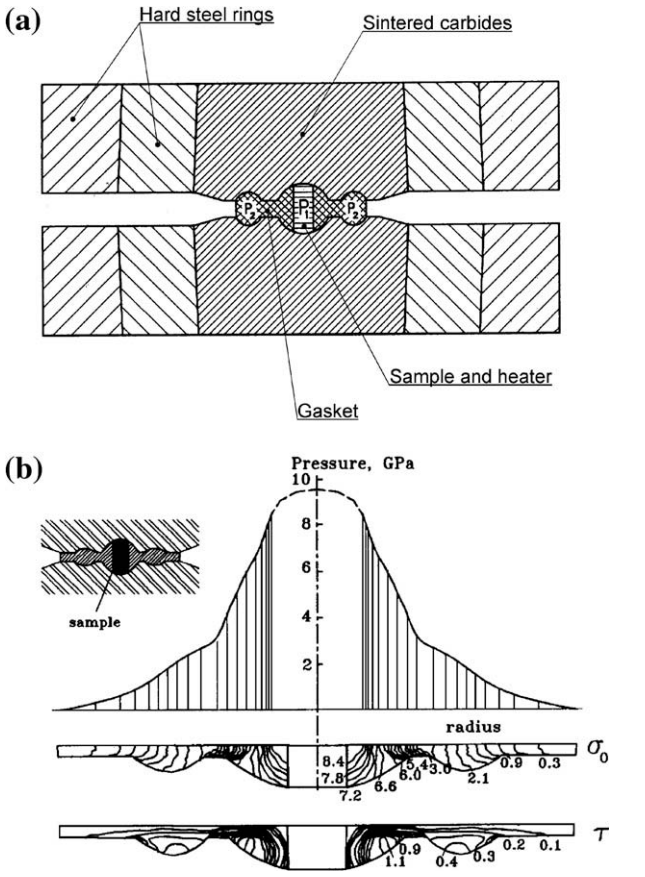

Fig. 1. Scheme of the Bridgmann type apparatus used for the densification of the TiC–TiB_2 and Ti–Al_2O_3–TiC powders obtained by SHS + quench, showing (a) the cross-section of anvil and sample and (b) the pressure distribution in the sample during plastic deformation of gasket.

cracks, and the corresponding temperature was identified as the critical temperature. The critical quenching temperature difference was determined as difference between the critical temperature and the temperature of the quenching bath. The temperature range considered for the thermal shock tests was between 250 and 800 °C. The procedure was carried out with 25 °C increments for both the material systems.

3. Results and discussion

Due to the high-pressure used in the sintering procedure, the presence of cracks is a usual problem in the samples densified by the HPHT method. The cracking of metal–ceramic or, especially, ceramic materials occurs as a result of residual micro and macro stresses overcoming the fracture strength of the material. The appearance of cracks is likely to occur during the cooling stage and the removal of external compaction loading. Moreover, fine powders are difficult to compact without cracks being characterized by a high specific surface area and significant amounts of gas absorbed on the particle surface. Finally, the recrystallisation, segregation and phase transitions developing during the HPHT process can result in cracking of the sintered sample. In order to prevent these cracking phenomena the HPHT process conditions have to be carefully controlled. Therefore, the pressure, temperature and duration of the sintering process were varied within a wide range. The HPHT sintering conditions investigated are summarized in Table 2 for both the TiC–TiB_2 and Ti–Al_2O_3–TiC composites.

Table 1
Phases detected by XRD in the materials densified by HPHT sintering and relative crystallite size calculated by Rietveld refinement.

Material	Phase	Crystallite size (nm)
TiC–TiB_2 (1380 °C, 240 s)	TiC	35
	TiB_2	90
Ti–Al_2O_3–TiC (1550 °C, 90 s)	α-Al_2O_3 (corundum)	72
	α-Ti	33
	TiC	37
	Ti_3Al	42

3.1. HPHT sintering of TiC–TiB_2

Regarding the TiC–TiB_2 composite, the samples characterized by the highest degree of densification and Young modulus were obtained at the lower value of pressure (4 GPa) and in the temperature range 1380–1520 °C, as shown in Fig. 2a and b, respectively. However some of the samples obtained under these conditions showed the presence of cracks. Composites with nearly full density and without cracks were obtained at the sintering temperature of 1380 °C.

As optimized sintering conditions, the TiC_{1-x}–TiB_2 compacts were sintered at a pressure of 4.0 ± 0.2 GPa and a temperature 1380 °C. The composites obtained under these optimized conditions were characterized by means of XRD analysis, hardness measurement and calculation of K_{Ic}, wear tests and thermal shock tests. The XRD pattern detected on the TiC–TiB_2 material showed the achievement of the desired titanium carbide and titanium diboride phases, as shown in Fig. 3. The broadening of the peaks indicated a small crystallite size as confirmed by Rietveld refinement reported in Table 1.

After the HPHT sintering process, a fine microstructure characterized by titanium diboride grains (dark grey phase) dispersed in a titanium carbide (light grey phase) matrix was observed in the case of the TiC–TiB_2 samples as shown in Fig. 4 and confirmed by EDX analysis. As can be observed in Fig. 4b, the sintered materials was characterized by the presence of submicrometric ceramic

Table 2
Summary of the composition and of the HPHT sintering conditions investigated.

Material theoretical composition	HPHT sintering conditions			Description of the densified material	Max sintered density (g/cm^3)
	Pressure (GPa)	Temp. (°C)	Time (s)		
TiC–38 wt.% TiB_2	4	1070	240	Cracks	4.59
		1190	240	Cracks	4.63
		1380	240	Ok	4.67
		1480	240	Sample broken	4.68
		1520	240	Sample broken	4.67
	7.7	1730	60	Cracks	4.59
		1730	90	Cracks	4.58
		2130	60	Ok	4.58
		2130	90	Microcracks	4.59
		2200	90	Net of microcracks	4.55
		2200	60	Net of microcracks	4.55
		2250	30	Cracks	4.40
		2250	60	Microcracks	4.55
		2250	90	Cracks	4.62
		2300	30	Cracks	4.54
		2320	60	Cracks	4.57
		2320	90	Microcracks	4.59
		2350	60	Cracks	4.54
		2370	60	Cracks	4.49
Ti–35 wt.% Al_2O_3–13 wt.% TiC	4	1220	120	Sample broken	4.51
	7.7	1550	90	Ok	4.57
		1730	90	Sample broken	4.57
		2010	30	Cracks	4.58
		2010	60	Sample broken	4.58
		2010	90	Sample broken	4.57
		2130	60	Cracks	4.58
		2130	90	Crack	4.58
		2250	60	Microcracks	4.58
		2250	90	Microcracks	4.57

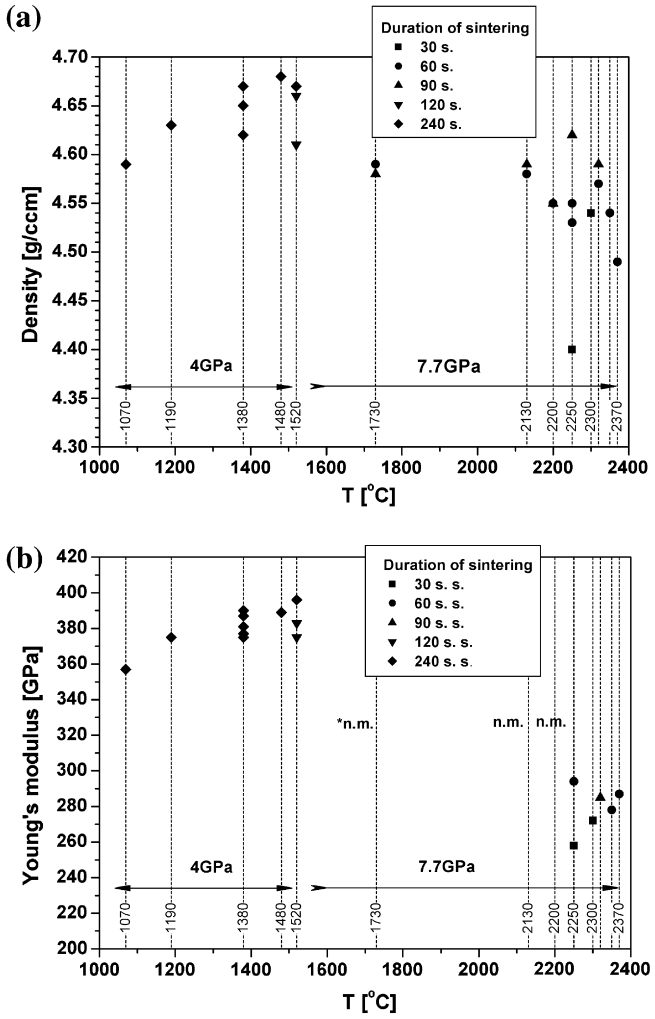

Fig. 2. Density (a) and Young modulus (b) of the TiC–TiB_2 composites sintered by HPHT under different processing conditions (temperature, pressure, time). (*n.m. – non measurable by ultrasonic method).

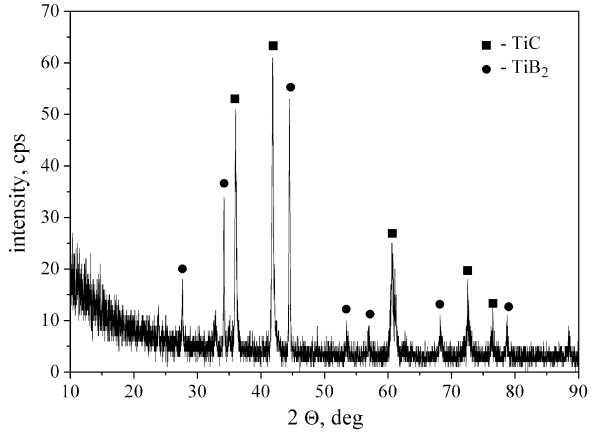

Fig. 3. XRD pattern for the TiC–TiB_2 composite sintered at 1380 °C for 240 s under a pressure of 4 GPa.

grains, down to 200 nm in size. The material densified according to the optimized conditions (240 s at 1380 °C under a pressure of 4 GPa) had a density higher than 98% of theoretical density.

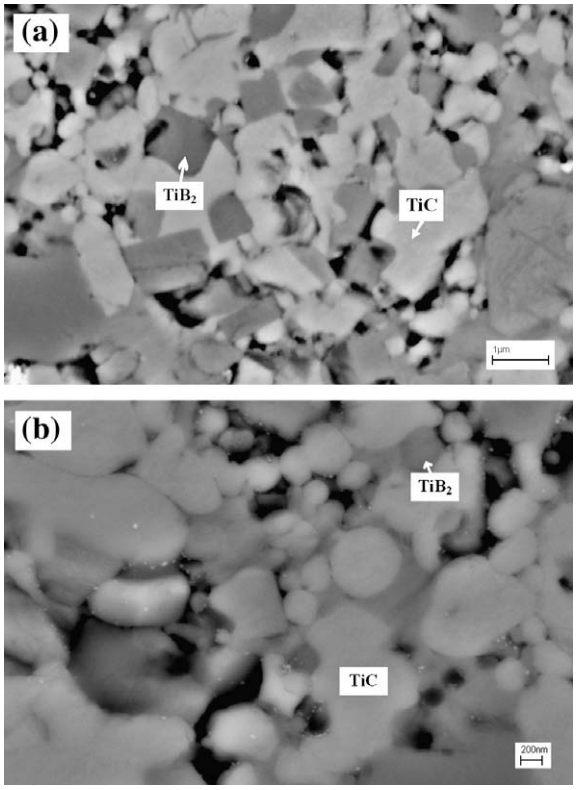

Fig. 4. Microstructure of the TiC–TiB_2 composite sintered by HPHT at 1380 °C for 240 s under a pressure of 4 GPa.

3.2. HPHT sintering of Ti–Al_2O_3–TiC

Regarding the Ti–Al_2O_3–TiC cermet, the highest values of density of Young modulus were obtained under the pressure of 7.7 GPa and in the temperature range between 1530 and 2250 °C approximately, as shown in Fig. 5a and b, respectively. In this case, the optimized Ti–Al_2O_3–TiC densified materials were obtained at the highest value of pressure (7.7 ± 0.2 GPa) and at the lowest temperature (1550 °C). The XRD pattern reported in Fig. 6 for the Ti–Al_2O_3–TiC densified material showed the presence of the main phases Ti, Al_2O_3 and TiC, with a limited content of intermetallic Ti_3Al phase (about 9 wt.% determined by Rietveld refinement). Also in this case the broadening of the peaks indicated a small crystallite size as confirmed by Rietveld refinement reported in Table 1.

The microstructural observations for the Ti–Al_2O_3–TiC composite showed a continuous titanium matrix with micrometric- or submicrometric-size phases constituted by Al_2O_3 and TiC (Fig. 7). By EDX analysis, the microstructure of the densified sample was characterized the presence of titanium, alumina, titanium carbide and small amounts of Ti_3Al confirming the phases shown in the X-ray pattern reported in Fig. 6, without any appreciable change from the original powder.

3.3. Mechanical properties of the sintered materials

The properties measured on the composites densified by HPHT sintering are summarized in Table 3. The TiC–TiB_2 material was characterized by high values of hardness, and a good combination of Young's modulus and acceptable fracture toughness predisposing this composite as valid material for applications such as cutting tools and wear parts. Regarding the Ti–Al_2O_3–TiC cermet, a very high value of hardness was measured considering the high content of metallic Ti (53 wt.%). In both the materials, the good properties

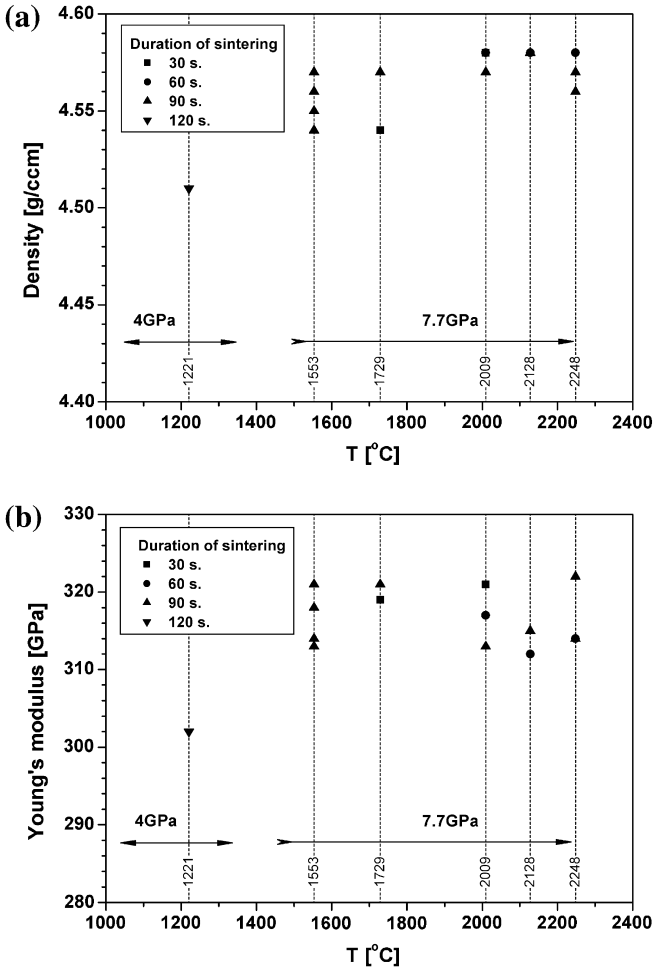

Fig. 5. Density (a) and Young modulus (b) of the Ti–Al_2O_3–TiC cermet sintered by HPHT under different processing conditions (temperature, pressure, time).

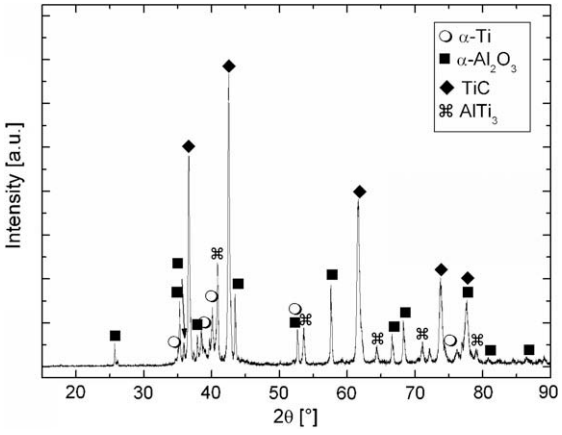

Fig. 6. XRD pattern for the Ti–Al_2O_3–TiC composite sintered at 1550 °C for 90 s under a pressure of 7.7 GPa.

measured can be correlated with the very fine microstructure observed on the HPHT sintered materials, showing the presence of submicronic grains as can be appreciated in Fig. 4b and Fig. 7b. Regarding this, the HPHT sintering method allowed an efficient densification without substantial coarsening of the microstructure. The grain size of the sintered materials reported in Fig. 8a and b was in fact comparable with the average particle size of the starting powders measured by laser granulometry, that was 2.8 μm [6] and 2.5 μm [5] for the TiC–TiB_2 and the Ti–Al_2O_3–TiC compositions, respectively.

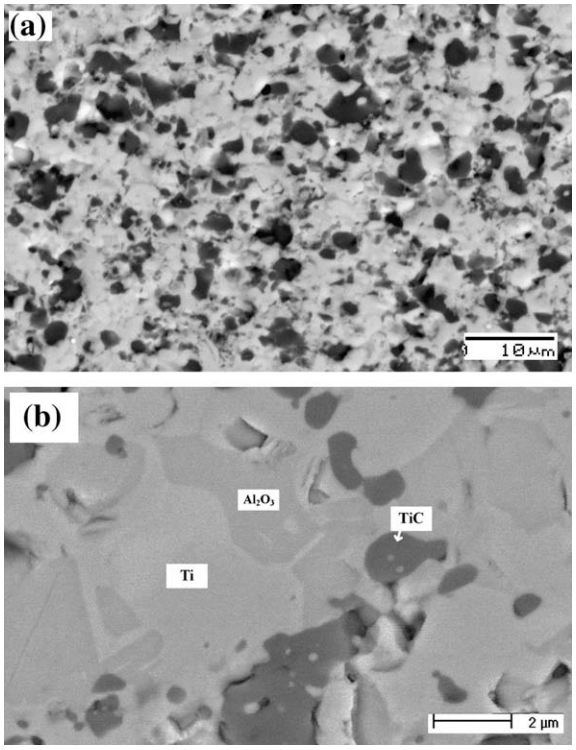

Fig. 7. Microstructure observed on the Ti–Al_2O_3–TiC composites sintered by HPHT at 1550 °C for 90 s under a pressure of 7.7 GPa.

The mechanism of fracture propagation after the indentation tests was investigated by microstructural observation by FESEM. Toughening mechanisms typical for composite materials were observed in both the ceramic and cermet systems. For the TiC–TiB_2 material, a significant crack deflection mechanism was observed, as shown in Fig. 8a. The presence of the diboride grains embedded in the matrix helps to dissipate the energy and to increase the fracture toughness of the material due to the elongated shape of the TiB_2 platelets.

Also in the Ti–Al_2O_3–TiC metal–ceramic composite, a positive effect was exerted by the ceramic grains embedded in the matrix that help to dissipate the energy of the propagating crack. In this material a toughening effect by crack bridging was observed as shown in Fig. 8b, due in this case to titanium bridges acting as a reinforcement slowing the fracture propagation and helping to increase the resistance to crack propagation.

3.4. Results and discussion on ball-on-disk wear test

The results of friction coefficient and temperature measurements during the wear tests by ball-on-disk method with Si_3N_4 balls are reported in Figs. 9 and 10 for the ceramic and the cermet materials, respectively. The coefficient of friction increased during the first 1000 cycles and then reached a constant value of about $\mu = 0.84$ for the TiC–TiB_2 samples. As shown in Fig. 9, the temperature in the contact area was slightly increased during the test up to a maximum value of about 42 °C after 3000 cycles. The coefficient of friction for Ti–Al_2O_3–TiC reached a lower value ($\mu = 0.76$ than that of the ceramic system, after 1500 cycles, as shown in Fig. 10. For the cermet material the value of friction coefficient resulted lower than 0.2 for the first 1000 cycles, and then increased almost linearly up to the maximum value. The reason for this

Table 3
Comparison between some properties relevant to wear-resistant applications for TiC–TiB_2 and Ti–Al_2O_3–TiC composites densified by HPHT sintering and those reported in selected literature works.

Material	Density	Young modulus E (GPa)	Vickers micro-hardness $HV_{0.3}$	Vickers hardness HV	Fracture toughness K_{Ic} (MPa $m^{1/2}$)	Thermal shock ΔT_c (°C)	Friction coefficient μ	Wear rate Wv (mm^3/Nm)	Calculated abrasive wear factor AWF	Ref.
TiC–38 wt.%TiB_2 by HPHT	4.68 g/cm^3	375	2267	2130 (HV_1)	4.6	300	0.84	2.2×10^{-6}	1.45	This work
Ti–35 wt.%Al_2O_3–13 wt.%TiC by HPHT	4.57 g/cm^3	313	1968	1770 (HV_1)	4.5	300	0.71	13.1×10^{-6}	1.27	This work
TiC–30 wt.%TiB_2	>99% TD	450	–	1900	5.3	350	–	–	1.26	[13]
Al_2O_3–30 wt.%TiC	–	–	–	–	–	150–200	–	–	1.22	[17]
SiAlON	–	–	–	–	–	–	–	–	1.21	[18]
WC–31 wt.%TiC–9 wt.%Co	>99% TD	–	–	1560	8.1	520	–	–	0.95	[19]

increase was probably the presence of hard ceramics particles detached during the test.

The morphology of the wear tracks formed in the HPHT sintered materials after the wear tests were observed by FESEM. The absence of microcracking was observed after sliding in the case of the TiC–TiB_2 material, as shown in Fig. 11a. For conventional ceramic materials the dominant mechanism of material removal is grain boundary fracture combined with lateral crack chipping. However, brittle fracture was not observed in the case of the ceramic composite sintered by HPHT. The wear mechanism observed in the TiC–TiB_2 material was abrasive wear, without crushing and chipping at the edge of the wear track. Only very fine powder-like wear debris was observed without any evidence of large block-like

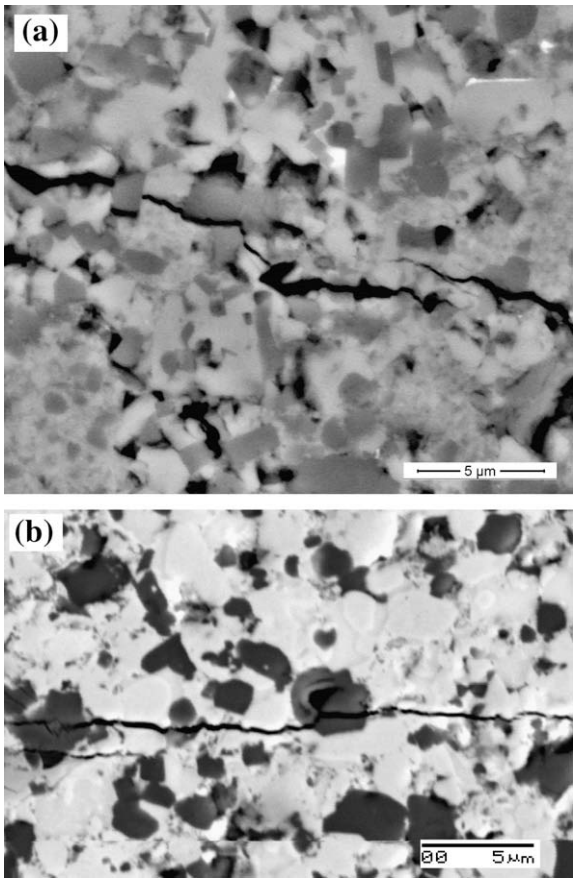

Fig. 8. SEM micrograph showing the mechanism of fracture propagation for the (a) TiC–TiB_2 composite sintered by HPHT (1380 °C, 240 s, 4 GPa) and for the (b) Ti–Al_2O_3–TiC cermet sintered by HPHT (1550 °C, 90 s, 7.7 GPa).

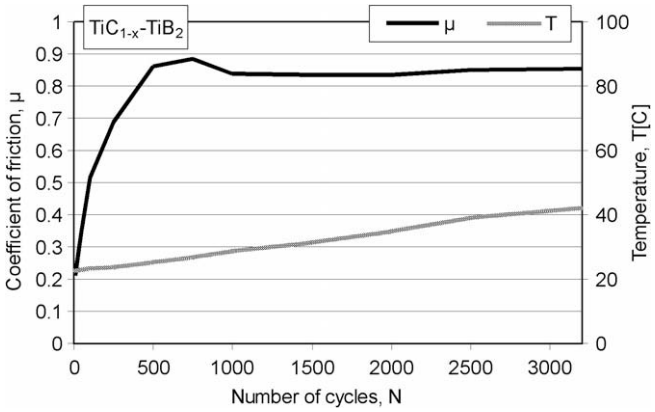

Fig. 9. Coefficient of friction and temperature measured in the contact zone between Si_3N_4 ball and specimen during ball-on-disk tests (3200 cycles; Fn = 1 N; v = 0.1 m/s; s = 100 m; R = 5 mm) for the TiC–TiB_2 composite sintered by HPHT.

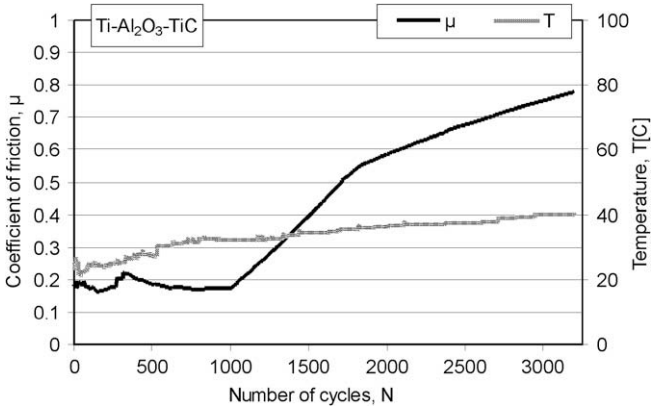

Fig. 10. Coefficient of friction and temperature measured in the contact zone between Si_3N_4 ball and specimen during ball-on-disk tests (3200 cycles; Fn = 1 N; v = 0.1 m/s; s = 100 m; R = 5 mm) for the Ti–Al_2O_3–TiC composite sintered by HPHT.

debris. The occurrence of these phenomena was probably due to the fine microstructure shown by the densified material. For the case of the Ti–Al_2O_3–TiC cermet, a sharp edge of the wear track after sliding was not observed (Fig. 11b) and single parallel abrasion marks appeared at the edge of the scar. As can be observed, the surface was worn mainly by the abrasion action of the hard slider. By FESEM observation the appearance of larger debris in the contact area was confirmed after 1000 cycles. The formation of this debris probably explains the increase in the coefficient of friction with the number of cycles shown in Fig. 10.

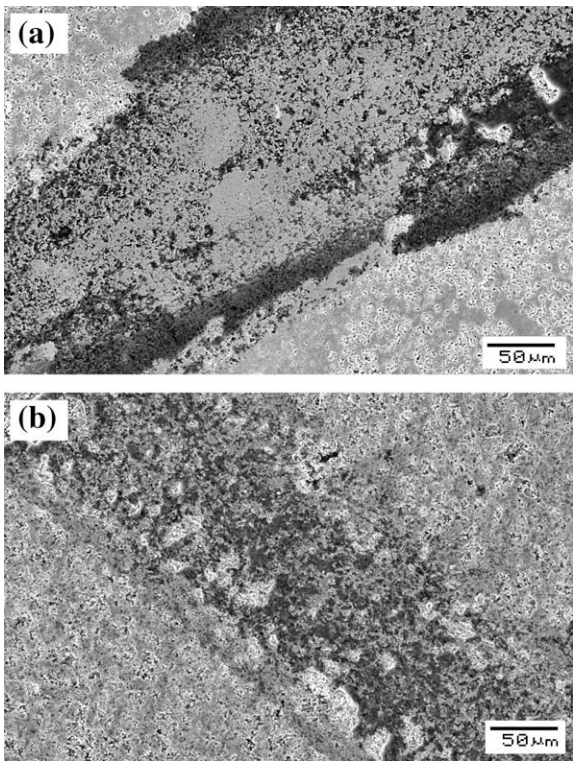

Fig. 11. Scanning electron micrograph of the worn contact area observed at FESEM after ball-on-disk tests on the (a) TiC–TiB_2 and (b) Ti–Al_2O_3–TiC materials sintered by HPHT.

To sum up, both the ceramic TiC–TiB_2 and cermet Ti–Al_2O_3–TiC materials sintered by HPHT showed a good combination of properties in terms of fine-grained microstructure, hardness, fracture toughness and Young modulus. These properties conferred the HPHT densified materials good wear and abrasion resistance, as confirmed by the low value of wear rate measured in both cases as reported in Table 3.

3.5. Discussion on wear factor

Concerning the use of this class of materials as cutting tools, Brodkin et al. [13] have carried out a comparison between TiC–TiB_2 composites and commercial materials based on the Abrasive Wear Factor (AWF) provided by Evans and Marshall [14] for the evaluation of the wear-resistance of ceramic and metal–ceramic materials. The wear factor can be computed from the fracture toughness (K_{Ic}), Young's modulus (E) and hardness (H) according to the following equation:

$$\mathrm{AWF} = \frac{K_{Ic}^{0.5} \cdot H^{1.43}}{E^{0.8}} \quad (1)$$

The higher the AWF, the higher the expected resistance of a ceramic material to abrasive wear. The results of the comparison reported by Brodkin et al. [13] showed that the wear factor of TiC–TiB_2 composites produced by Transient Plastic Phase Processing TPPP (AWF = 1.26) favourably compares to commercial Al_2O_3–TiC (1.22) and SiAlON (1.21) cutting tool materials. The good wear-resistance of the material was also confirmed from data obtained from abrasive erosion tests by the same authors [13]. It was observed that the wear rate of the TPPP TiC–TiB_2 based composites was comparable to that of SiAlON and WC–Co cutting tool materials. The comparison was extended to the TiC–TiB_2 materials densified by HPHT reported in this work. As can be seen from the data reported in Table 3, the materials developed in this work showed a value of Abrasive Wear Factor significantly higher than all the other competing materials considered in the comparison. As for the Ti–Al_2O_3–TiC cermet, the wear behavior of the material sintered by HPHT favourably compared to that reported in the literature for titanium alloys like e.g. Ti–48Al–2Cr–2Nb for which a value of wear rate of 14×10^{-6} mm^3/Nm has been measured [15]. In agreement with the sliding wear phenomena of ceramics and metal–ceramic composites, the type of wear observed in the developed materials could be classified as "mild wear" [16].

This excellent combination of properties together with the good thermal shock resistance make the developed materials valid candidates for wear-resistant applications, such as cutting tools for machining difficult-to-machine materials (e.g. Ni-based alloys) for the TiC–TiB_2 ceramic and wear parts (such as gearbox components, transmission camshaft, etc. for the automotive sector) for the Ti–Al_2O_3–TiC cermet.

4. Conclusions

Metastable nanostructured TiC–TiB_2 ceramic and Ti–Al_2O_3–TiC cermet powders produced by SHS + quench were successfully densified by high-pressure high-temperature HPHT sintering. The TiC–TiB_2 ceramic system was successfully sintered at 1380 °C for 240 s under a pressure of 4 GPa. A higher pressure of 7.7 GPa and a temperature of 1550 °C for 90 s was necessary for the Ti–Al_2O_3–TiC cermet. The rapid sintering cycles allowed by the HPHT method were effective in limiting the grain growth and in retaining a fine-grained microstructure during sintering. In both cases, the resulting composite structure was fine-grained and fully dense. The densified composite materials showed good properties in terms of Young modulus, hardness, toughness, wear rate and thermal shock resistance, which are generally higher than those of similar available state-of-the-art materials. The wear properties (friction coefficient and wear rate) of the developed bulk materials are promising for future technological applications. Brittle fracture mechanisms typical for ceramic materials were not observed in the TiC–TiB_2 composite. The predominant wear mechanism was abrasive for both materials with no evidence of crushing and chipping thanks to the fine microstructure obtained.

Acknowledgements

This work was carried out in the framework of the FP6 STREP project NAMAMET "Processing of Nanostructured Materials through Metastable Transformations" supported by the European Commission under the contract NMP3–CT–2004–001470.

References

[1] Wen G, Li SB, Zhang BS, Guo ZX. Reaction synthesis of TiB_2–TiC composites with enhanced toughness. Acta Mater 2001;49:1463–70.
[2] Fan R, Liu B, Zhang J, Bi J, Yin Y. Kinetic evaluation of combustion synthesis $3TiO_2 + 7Al \rightarrow 3TiAl + 2Al_2O_3$ using non-isothermal DSC method. Mater Chem Phys 2005;91:140–5.
[3] Kear BH, Kalman Z, Sandagi RK, Skandan G, Colaizzi J, Mayo WE. Plasma-sprayed nanostructured Al_2O_3/TiO_2 powders and coatings. J Therm Spray Technol 2000;9:483–7.
[4] Vallauri D, López Y, DeBenedetti B, Amato I. Nanocomposite TiC–TiB_2 powders by SHS through metastability approach. Adv Sci Technol 2006;45:1005–10.
[5] Mas-Guindal MJ, Benko E, Rodriguez MA. Nanostructured metastable cermets of Ti–Al_2O_3 through activated SHS reaction. J Alloy Compd 2008;454:352–8.
[6] Vallauri D, Atías Adrián IC, Deorsola FA, Amato I, DeBenedetti B. Metastability route to obtain nanocomposites by SHS. Int J SHS 2006;15(2):169–79.
[7] Liao SC, Chen YJ, Kear BH, Mayo WE. High pressure/low temperature sintering of nanocrystalline alumina. Nanostruct Mater 1998;10:1063–79.
[8] Liao SC, Pae KD, Mayo WE. Retention of nanoscale grain size in bulk sintered materials via a pressure-induced phase transformation. Nanostruct Mater 1997;8:645–56.

[9] Liao SC, Colaizzi J. Refinement of nanoscale grain structure in bulk titania via a transformation-assisted consolidation (tac) methods. J Am Ceram Soc 2000;83:2163–9.
[10] Skandan G, Yao R, Kear BH, Qiao YF, Liu L, Fisher TE. Multimodal powders: a new class of feedstock material for thermal spraying of hard coatings. Scripta Mater 2001;44:1699–702.
[11] Merzhanov AG. Self-propagating high-temperature synthesis: twenty years of search and findings. In: Munir ZA, Holt JB, editors. Combustion and plasma synthesis of high-temperature materials. New York: VCH; 1990. p. 1–53.
[12] Niihara K, Morena R, Hasselman DPH. Evaluation of K_{Ic} of brittle solids by the indentation method with low crack-to-indent ratios. J Mat Sci Lett 1982;1:13–6.
[13] Brodkin D, Zavaliangos A, Kalidindi S, Barsoum M. Ambient- and high-temperature properties of titanium carbide–titanium boride composites fabricated by transient plastic phase processing. J Am Ceram Soc 1999;82:665–72.
[14] Evans AG, Marshall DB. Wear mechanisms in ceramics. In: Rigney DA, editor. ASM fundamentals of friction and wear of materials. Metals Park, OH: ASM International; 1981. p. 439–52.
[15] Miyoshi K, Sanders JH, Hager Jr CH, Zabinski JS, Vander Wal RL, Andrews R, et al. Wear behavior of low-cost, lightweight TiC/Ti–6Al–4V composite under fretting: effectiveness of solid-film lubricant counterparts. Tribol Int 2008;41:24–33.
[16] Adachi K, Kato K, Chen N. Wear map of ceramics. Wear 1997;203–204:291–301.
[17] Wayne SF, Buljan ST. The role of thermal shock on tool life of selected ceramic cutting-tool materials. J Am Ceram Soc 1989;72:754–60.
[18] Mehrotra PK. Evaluation of engineering ceramics for wear applications. In: Ludema KC, editor. Wear of materials, vol. I. New York: ASME; 1987. p. 301–12.
[19] Upadhyaya GS. Materials science of cemented carbides – an overview. Mater Des 2001;22:483–9.